Article

Cowpea Mosaic Virus Nanoparticle Vaccine Candidates Displaying Peptide Epitopes Can Neutralize the Severe Acute Respiratory Syndrome Coronavirus

Oscar A. Ortega-Rivera, Sourabh Shukla, Matthew D. Shin, Angela Chen, Veronique Beiss, Miguel A. Moreno-Gonzalez, Yi Zheng, Alex E. Clark, Aaron F. Carlin, Jonathan K. Pokorski, and Nicole F. Steinmetz*

Cite This: https://doi.org/10.1021/acsinfecdis.1c00410

Read Online

ACCESS | Metrics & More | Article Recommendations | Supporting Information

ABSTRACT: The development of vaccines against coronaviruses has focused on the spike (S) protein, which is required for the recognition of host-cell receptors and thus elicits neutralizing antibodies. Targeting conserved epitopes on the S protein offers the potential for pan-beta-coronavirus vaccines that could prevent future pandemics. We displayed five B-cell epitopes, originally identified in the convalescent sera from recovered severe acute respiratory syndrome (SARS) patients, on the surface of the cowpea mosaic virus (CPMV) and evaluated these formulations as vaccines. Prime-boost immunization of mice with three of these candidate vaccines, CPMV-988, CPMV-1173, and CPMV-1209, elicited high antibody titers that neutralized the severe acute respiratory syndrome coronavirus (SARS-CoV) *in vitro* and showed an early Th1-biased profile (2−4 weeks) transitioning to a slightly Th2-biased profile just after the second boost (6 weeks). A pentavalent slow-release implant comprising all five peptides displayed on the CPMV elicited anti-S protein and epitope-specific antibody titers, albeit at a lower magnitude compared to the soluble formulations. While the CPMV remained intact when released from the PLGA implants, processing results in loss of RNA, which acts as an adjuvant. Loss of RNA may be a reason for the lower efficacy of the implants. Finally, although the three epitopes (988, 1173, and 1209) that were found to be neutralizing the SARS-CoV were 100% identical to the SARS-CoV-2, none of the vaccine candidates neutralized the SARS-CoV-2 *in vitro* suggesting differences in the natural epitope perhaps caused by conformational changes or the presence of *N*-linked glycans. While a cross-protective vaccine candidate was not developed, a multivalent SARS vaccine was developed. The technology discussed here is a versatile vaccination platform that can be pivoted toward other diseases and applications that are not limited to infectious diseases.

KEYWORDS: SARS, SARS-CoV-2, coronavirus, CPMV, peptide-based vaccine, slow-release formulation
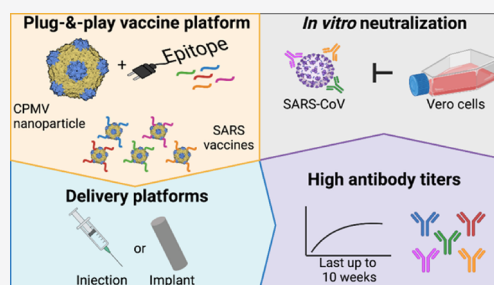
Coronaviruses are enveloped viruses with a positive-sense single-stranded RNA genome encoding up to four proteins.[1] There are four major branches assigned with the letters alpha, beta, gamma, and delta, and seven species are known to infect humans.[2] Four of these (two alpha- and two beta-coronaviruses) cause mild cold-like symptoms,[3] whereas the other three (all beta-coronaviruses) have been responsible for outbreaks of life-threatening infections in the last 20 years. The first was the severe acute respiratory syndrome coronavirus (SARS-CoV),[4] which emerged in China in 2002 and infected ~8500 people globally, causing ~800 deaths before the last cases were reported in 2004. The second was the Middle East respiratory syndrome coronavirus (MERS-CoV),[5] which emerged in Saudi Arabia in 2012 and has infected more than 2500 people and killed ~880 thus far, with sporadic cases still reported due to the disease reservoir in camels. The most recent was the severe acute respiratory syndrome coronavirus 2 (SARS-CoV-2), which emerged in

China in 2019 and is the cause of the current pandemic of coronavirus disease 2019 (COVID-19).[6] This virus has infected more than 179 million people thus far and has caused almost 4 million deaths.[7]

Although vaccine development programs have been launched for SARS and MERS, the massive global impact of COVID-19 has driven much of the research community to focus on this disease. At the time of writing, 18 COVID-19 vaccines have already been approved around the world, two based on the novel approach of mRNA-laden lipid nano-particles, two subunit vaccines, five based on viral vectors, and

Table 1. B-Cell Epitopes from the SARS-CoV-2/SARS-CoV S Proteins

location (name)[a]	sequence	solubility[b]	pI	length	identity %[c]	source
310-317	KGIYQTSN	good	9.5	8	100	24 and 37
346-362	ATRFASVYAWNRKRISN	good	11.8	17	76	this work
972-988	AISSVLNDILSRLDKVE	good	4.2	17	100	24 and 38
1157-1173	KNHTSPDVDLGDISGIN	good	4.0	17	100	24 and 38
1182-1209	EIDRLNEVAKNLNESLIDLQEL	good	3.7	22	100	24 and 39

[a]Each peptide is named according to the C-terminal residue position and is color-coded. [b]Theoretical solubility in water. [c]Compared to the SARS-CoV.

the remainder using the conventional approach of virus inactivation.[8] More than 300 further vaccine candidates have entered preclinical development, including several produced in plants.[9]

The development of vaccines against all three viruses has focused on the spike (S) protein, which projects from the viral envelope and is required for the recognition of host-cell receptors that mediate viral entry.[10−13] In the case of the SARS-CoV and SARS-CoV-2, this receptor is human angiotensin converting enzyme 2 (hACE2),[14,15] whereas the MERS-CoV receptor is dipeptidyl peptidase 4 (CD26/hDPP4).[16] The most potent neutralizing antibodies developed thus far recognize the receptor-binding domain (RBD) of the S protein and directly interfere with receptor−ligand binding.[17] The RBD contains multiple neutralizing antibody epitopes but few immunodominant epitopes that could induce harmful immune responses such as antibody-dependent enhancement of viral infection and therefore appears to be a better vaccine candidate than the entire S protein.[18] Indeed, the RBD induces a higher titer of neutralizing antibodies than the S1 ectodomain,[19] but the RBD alone has low immunogenicity. This can be addressed by the simultaneous administration of adjuvants[20] combined with alternative strategies such as RBD dimers[21] or the presentation of multiple epitopes on virus-like particles (VLPs) and nanoparticles.[22]

Given that the S proteins from the SARS-CoV and SARS-CoV-2 share 77% sequence identity and recognize the same receptor[23] and the nucleocapsid (N) and S proteins of the viruses share 27 T-cell epitopes and 49 B-cell epitopes,[24] groups developing vaccines have investigated the potential for cross-protection.[25] Several of these studies have shown that sera or purified IgG from animals immunized with the S protein or the RBD of one virus can neutralize the other.[26−31] This suggests that vaccine candidates targeting the S protein, and more specifically the RBD, have the potential to be developed as pan-beta-coronavirus vaccines that elicit broadly neutralizing antibodies, which can maintain efficacy against coronavirus divergence, thus offering a potential strategy to prevent/combat future pandemics caused by this virus group.[32,33]

We set out to engineer a broadly effective vaccine against beta-coronaviruses by selecting five B-cell epitopes, four with 100% sequence identity between the SARS-CoV and SARS-CoV-2,[24] which were identified by immunoinformatic mapping[34−36] and validated as immunogenic or reactive to sera from convalescent SARS-CoV patients.[37−39] These peptide epitopes were conjugated to the surface of a plant virus (cowpea mosaic virus, CPMV), a strategy that has proven to be effective in previous studies for the development of potent vaccine candidates based on plant viral nanoparticles (VNPs) displaying multiple copies of the epitope to elicit an enhanced immune response.[40] Such VNP-based vaccines can

be manufactured via propagation in host plants with relatively lower technological and financial burden. Plants have been used to produce vaccine candidates for 30 years, and several companies are developing COVID-19 vaccines in plants including one based on self-assembling S-protein virus-like particles (VLPs) that has completed phase I clinical trials[22] and is now beginning phase II/III, with millions of doses already ordered by the Canadian Government.[41]

Here, we report how plant VNPs based on the CPMV conjugated with B-cell epitopes can be developed as a vaccine candidate for beta-coronavirus neutralization. Soluble CPMV vaccine candidates were evaluated using prime-boost immunization. The ongoing COVID-19 pandemic highlights the need for vaccine candidates and delivery devices that overcome cold chain requirements and are effective after a single administration. Therefore, we also formulated the CPMV vaccine candidates as a slow-release polymer implant prepared by hot-melt extrusion, a highly scalable process technology suited for epidemic or pandemic response. Our previous research showed that VNPs can withstand hot-melt extrusion, yielding slow-release polymer melts that release structurally intact and biologically active VNPs; in previous work, virus-like particles (VLPs) derived from a bacteriophage were considered;[42−46] here, we apply these technologies to the plant virus CPMV.

◼ RESULTS

Selection of B-Cell Epitopes. We selected five B-cell epitopes that were previously identified as targets of antibodies from sera of convalescent patients with SARS[37,38] or that were shown to neutralize the SARS-CoV when used as a source of antigens in a vaccine candidate.[39] Four of the epitopes shared 100% sequence identity between the SARS-CoV and SARS-CoV-2 S proteins, whereas epitope 362 showed 76% sequence identity between the viruses (Table 1).[24] Two of the epitopes (317 and 362) are located within or immediately adjacent to the RBD, which binds the receptor ACE2, whereas the other three are located in the HR1/HR2 stalk region of the S2 subunit, which is required for cell fusion (Figure 1).[47,48]

Preparation of CPMV-Based Vaccine Candidates. Each of the five B-cell epitopes was synthesized as a synthetic peptide with N-terminal cysteine followed by a GGG linker for conjugation to CPMV particles using a two-step procedure (Figure 2A,B). The vaccine candidates were purified by ultracentrifugation and characterized by DLS, TEM, and SDS-PAGE under reducing conditions to confirm the structural integrity and determine the degree of antigen incorporation (Figure 2C−E). SDS-PAGE analysis indicated that each VNP presented 46−52 peptides (Figure 2C). Efficiency of the conjugations varied by peptide—it was interesting to note the band laddering effect for the CPMV-1173 and CPMV-1209 (Figure 2C lanes 2 and 3), which indicates that more than one peptide was conjugated per coat protein; this is possible
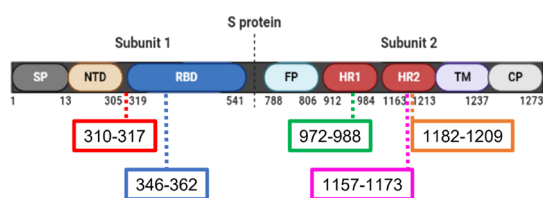
Figure 1. SARS-CoV-2 S protein domain map. Subunits and domains are not shown to scale. The positions of B-cell epitopes are shown, and the color code matches Table 1. SP = signal peptide; NTD = N-terminal domain; RBD = receptor-binding domain; FP = fusion peptide; HR1 = heptad repeat 1; HR2 = heptad repeat 2; TM = transmembrane domain; CP = cytoplasmic domain.

because the S and L proteins are both present with multiple lysine side chains (2 per S and 3 per L).[49] Nevertheless, the overall peptide loading per CPMV was comparable among the five vaccine candidates. DLS and TEM confirmed that the VNPs were monodisperse before and after conjugation (Figure 2D,E) and that their hydrodynamic diameter increased only marginally from 30.4 nm for the wild-type particles to 32.7 nm for each vaccine candidate (Figure 2D,E). We also observed no clouding of the suspension; therefore, data indicate stable formulations free of protein aggregation.

Immunogenicity of the CPMV-Based Vaccine Candidates. All five vaccine candidates were injected into mice with a prime-boost-boost schedule, and antibodies against all five peptides were recovered (Figure 3A,B). Endpoint IgG titers against CPMV-317 increased steadily, from 1:560 (week 2) to 1:6160 (week 4), 1:100,480 (week 6), and 1:105,600 (week 10). For CPMV-988, IgG titers were already high after 2 weeks (1:11,520) and then gradually declined to 1:10,240 (week 4), 1:7680 (week 6), and 1:8320 (week 10). For CPMV-1173, IgG titers initially increased from 1:3840 (week 2) to 1:18,560 (week 4) and 1:92,160 (week 6) but then declined to 1:81,920 (week 10). Similarly, the IgG titers against CPMV-1209 increased from 1:2560 (week 2) to 1:14,080 (week 4) and 1:35,840 (week 6) before falling to 1:19,200 (week 10). Finally, endpoint IgG titers against CPMV-362 remained relatively constant at 1:12,800 (week 2), 1:25,600 (week 4), 1:11,520 (week 6), and 1:12,800 (week 10), albeit with a transient increase at week 4. As expected, free peptides were not immunogenic, and no IgG titers were detected after priming and two boosts (Figure 3C).

Ig isotypes (Figure S1) and IgG subclasses (Figure 3D) were investigated to determine whether the candidates induced a Th cell response based on the IgG1/IgG2a ratio (values <1 defined as Th1-biased and values >1 defined as Th2-biased). After priming (week 2), all candidates except CPMV-362 showed a Th1-biased profile, but this switched to a Th2-biased profile after the second boost (Figure 3D).

Immunoreactivity of the Serum against the SARS-CoV-2 S Protein. The plasma samples used to determine IgG titers and isotype profiles were also used to provide a preliminary indication of immunoreactivity against the SARS-CoV-2 S protein. ELISA experiments revealed that IgG from the plasma samples taken on weeks 2, 4, and 6 from all mice injected with the vaccine candidates was able to recognize the SARS-CoV-2 S protein (Figure 4A). Four of the candidates showed week-2 titers of 1:25,000, the exception being CPMV-362 with a titer of only 1:5000. By week 6, three of the candidates achieved titers of 1:125,000, with CPMV-1173 slightly lower at 1:105,000 and CPMV-1209 the lowest at

1:85,000. Plasma from mice injected with the free peptides did not bind to the S protein (Figure 4B).

Analysis of T-Cell Responses to the Vaccine Candidates. The T-cell responses to the vaccine candidates were evaluated using an ELISpot assay following the vaccination of mice with a single dose (prime) or the complete schedule (prime and two boosters). Splenocytes were collected from immunized animals and stimulated with each peptide (317, 988, 1173, 1209, or 362), with a normal cell culture medium as a negative control or with the CPMV plus PMA and ionomycin as a positive control. ELISpot analysis of splenocytes from animals receiving the vaccine candidates (CPMV-317, CPMV-988, CPMV-1173, CPMV-1209, or CPMV-362) did not show the presence of IFN-γ spot-forming colonies (SFCs) when stimulated with the matching peptide regardless of whether the VNPs were delivered as a single dose (Figure 5A) or three doses (Figure 5B), which supports evidence of a Th2-biased profile provided by the IgG subclass ratios (Figure 3D). However, we also observed no significant increase in the abundance of IL-4 SFCs following stimulation with the matching peptides (Figure 5A,B), indicating that basal levels of IL-4 are sufficient for a Th2-biased response. Splenocytes stimulated with the CPMV resulted in the appearance of more IFN-γ SFCs (Figure 5A,B), demonstrating that the CPMV itself triggers a Th1 response as previously reported.[50] As expected, stimulation with PMA and ionomycin triggered an increase in both IFN-γ and IL-4 SFCs. Representative images from each vaccine group and the various stimulants are shown in Figure 5C.

Neutralization of the SARS-CoV and SARS-CoV-2. Having confirmed the presence of IgG recognizing the peptide epitopes and the S protein following immunization with all five vaccine candidates, we tested the plasma samples for the presence of neutralizing antibodies against the SARS-CoV and SARS-CoV-2. Pooled plasma from each vaccinated group was preincubated separately with each virus and then added to Vero 76 cells to evaluate the impact on virus cytopathicity. The EC_{50} and CC_{50} were determined visually and from neutral red absorbance readings and were used to calculate the SI_{50} with values ≥10 indicating neutralizing activity. The neutralization titers are reported in Table 2. Only the plasma sample from mice injected with CPMV-988, CPMV-1173, and CPMV-1209 was able to neutralize the SARS-CoV, with similar neutralization titers but a slightly higher SI_{50} value in the case of CPMV-1209 (Table 2). None of the samples were able to neutralize the SARS-CoV-2 in the same assay (Table 2).

Analysis of Pentavalent Vaccine Implants. The five CPMV-based vaccine candidates were formulated as a cylindrical implant by hot-melt extrusion using a mixture of the pentavalent VNPs, PLGA, and PEG8000 (10:75:15, w/w/w). The dose loaded for each pentavalent implant (300 μg of each CPMV vaccine) was equivalent to the three-dose (100 μg each dose; prime-boost-boost) soluble injection schedule. The same approach was used to formulate CPMV-Cy5 VNPs (the characterization of CPMV-Cy5 is reported in the Supporting Information, Figure S2) to trace their slow-release profiles post-implantation and their fate during lymph node drainage. Lymph nodes were collected every week for 5 weeks from animals carrying the CPMV-Cy5 implant (Figure 6A), and blood was taken every 2 weeks for 6 weeks from animals carrying the pentavalent implant (Figure 6B). We collected cervical, axillary, and inguinal lymph nodes, as shown in Figure 6C. The gradual release of CPMV-Cy5 from the implant over 5
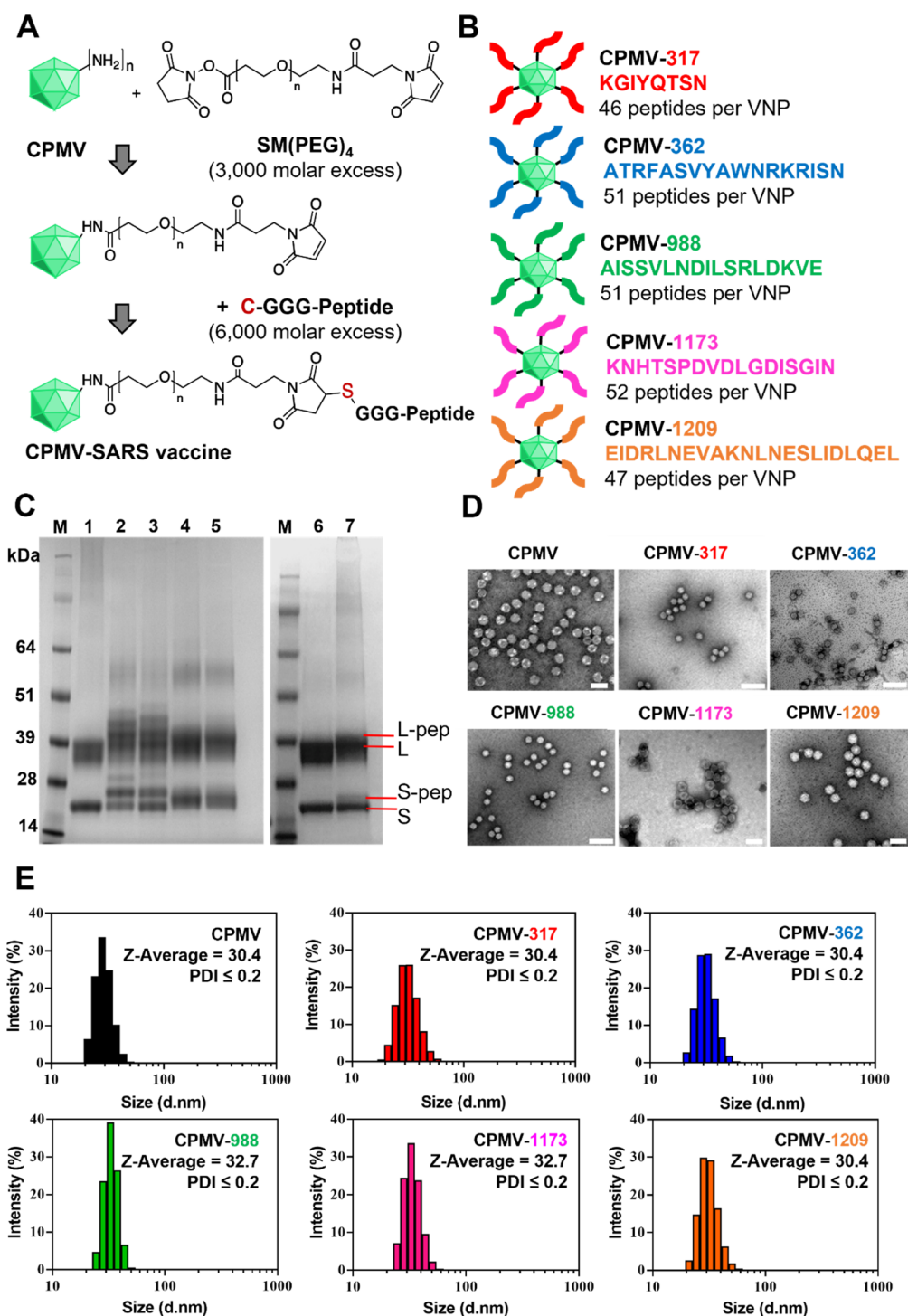
Figure 2. Synthesis and characterization of CPMV vaccine candidates. (A) Two-step conjugation of B-cell epitope peptides 317, 362, 988, 1173, and 1209 to the wild-type CPMV. (B) CPMV vaccine candidates and the number of peptides displayed per VNP. (C) SDS-PAGE: lane M = size markers; lanes 1 and 6 = wild-type CPMV; lane 2 = CPMV-1173; lane 3 = CPMV-1209; lane 4 = CPMV-317; lane 5 = CPMV-988; lane 7 = CPMV-362. S = small capsid protein; S-pep = small capsid protein conjugated with a peptide; L = large capsid protein; L-pep = large capsid protein conjugated with a peptide. (D) TEM images of the negatively stained wild-type CPMV and the vaccine candidates. For the CPMV, CPMV-1173, and CPMV-1209, the white bar = 50 nm; for CPMV-317, CPMV-988, and CPMV-362, the white bar = 100 nm. (E) Particle size determined by DLS, showing the Z-average diameter (d (nm)) and the polydispersity index (PDI) for each candidate.

weeks was confirmed by the progressive loss of fluorescence from the implantation zone (Figure 6D).

In addition to the fluorescence imaging studies of CPMV-Cy5/PLGA implants, we also determined whether the CPMV was intact when released from the implants *in vitro*. The

CPMV recovered from implants was subjected to DLS sizing experiments and TEM imaging. DLS and TEM are consistent with intact and monodisperse nanoparticles being released from the implants with sizes measuring ~30 nm and indistinguishable features compared to the CPMV (Figure S3).
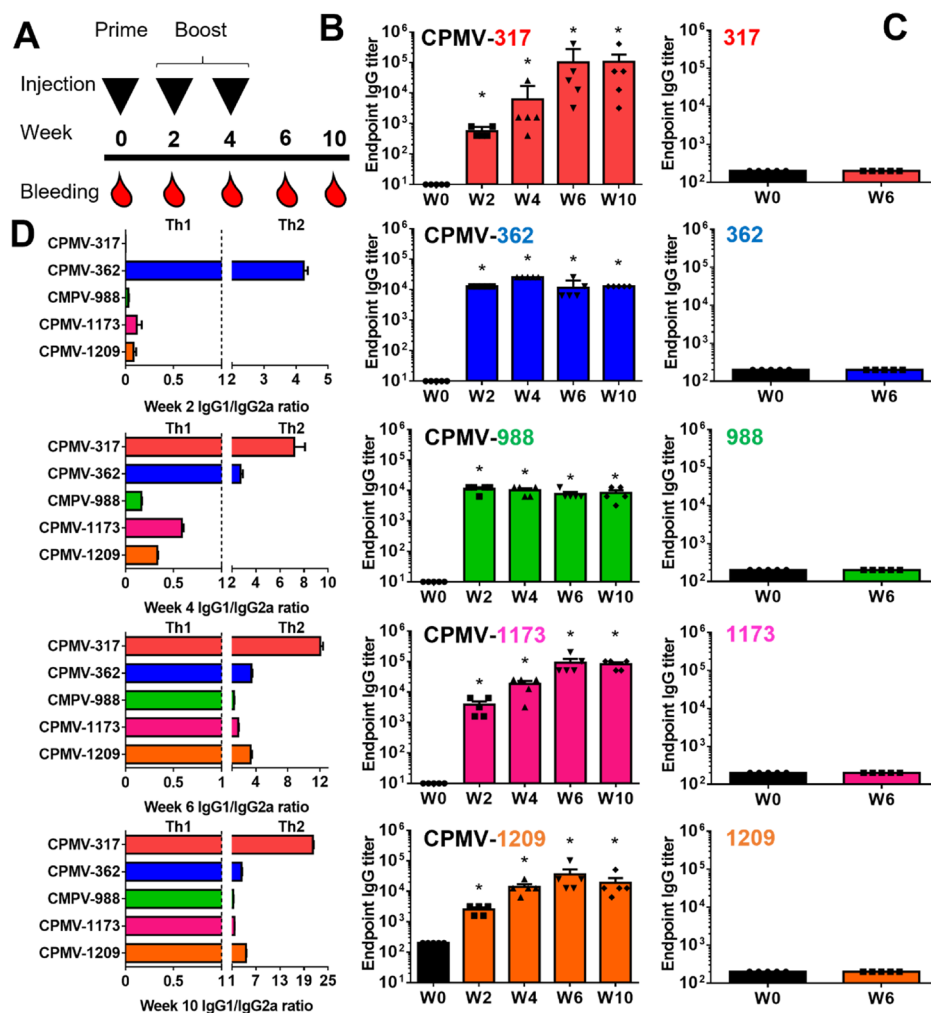
Figure 3. Analysis of vaccine candidate immunogenicity by ELISA. (A) Immunization schedule using 100 μg of each vaccine candidate or 5 μg of the free peptide per injection (n = 5 mice per group). (B) Endpoint IgG titers from animals vaccinated with red = CPMV-317, green = CPMV-988, pink = CPMV-1173, yellow = CPMV-1209, or blue = CPMV-362, at various times in weeks (W0–W10) after the first immunization (W0 corresponds to plasma collected prior to the first immunization). (C) Endpoint IgG titers from animals vaccinated with free peptides (color code identical to panel (B)). (D) IgG isotype profile (IgG1/IgG2a ratio) 0–10 weeks after the first immunization (values <1 defined as Th1-biased and values >1 defined as Th2-biased). Statistical significance: *p < 0.0001 vs W0.

In vivo imaging experiments show that the loss of fluorescence from the CPMV-Cy5 implant matched the gradual increase in antibody titers against all five peptides (Figure 6E–I) and against the SARS-CoV-2 S protein (Figure 6J) from the pentavalent implant, confirming that the released VNPs are immunogenic and stimulate the humoral immune response. The antibody titers against the CPMV carrier itself were 1:6400 for the pentavalent CPMV implant and CPMV-Cy5 implant but 1:204,800 for all individually soluble injected CPMV vaccines (CPMV-317, CPMV-362, CPMV-988, CPMV-1173, and CPMV-1209) (Figure S4). Furthermore, the IgG titers achieved by the pentavalent implant (Figure 6E–I) were reported for each individual vaccine (CPMV-317, CPMV-362, CPMV-988, CPMV-1173, and CPMV-1209) over the different time points (week 0 to week 6). For CPMV-317, titers were 1:1600, 1:7200, and 1:7200 (weeks 2, 4, and 6, respectively); for CPMV-362, titers were 1:1600, 1:3200, and 1:4160 (weeks 2, 4, and 6, respectively); for CPMV-988, titers were 1:1120, 1:2400, and 1:1440 (weeks 2, 4, and 6, respectively); for CPMV-1173, titers were 1:1040, 1:6080, and 1:10880 (weeks 2, 4, and 6, respectively); and for CPMV-

1209, titers were 1:2080, 1:4000, and 1:3680 (weeks 2, 4, and 6, respectively). The antibody titer at week 6 against the SARS-CoV-2 S protein was 1:25000, which corresponds to all the IgG generated against the five epitopes used in the CPMV vaccines that can bind the S protein.

The fate of CPMV-Cy5 particles was traced in more detail by analyzing sections of cervical, axillary, and inguinal lymph nodes on days 0, 7, 14, and 28 using antibodies against the markers CD4 (T cells), CD45R (B cells), and CD11c (dendritic cells) for colocalization (Figure 7). On day 0, we observed the presence of B-cell-rich zones (CD45R, red panel) surrounded by T cells (CD4, blue panel) and a random distribution of dendritic cells (CD11c, green panel) within the T-cell-rich zone in all lymph nodes. No background was observed from the Cy5 channel (CPMV-Cy5, gray panel). On day 7, we detected the presence of CPMV-Cy5 in the cervical lymph nodes, including the formation of germinal centers (Figure 7, merged panel). A weak signal was also detected in the axillary lymph node, but the presence of germinal centers was not clear. On day 14, CPMV-Cy5 was present in all lymph nodes, and germinal centers were clearly present in axillary
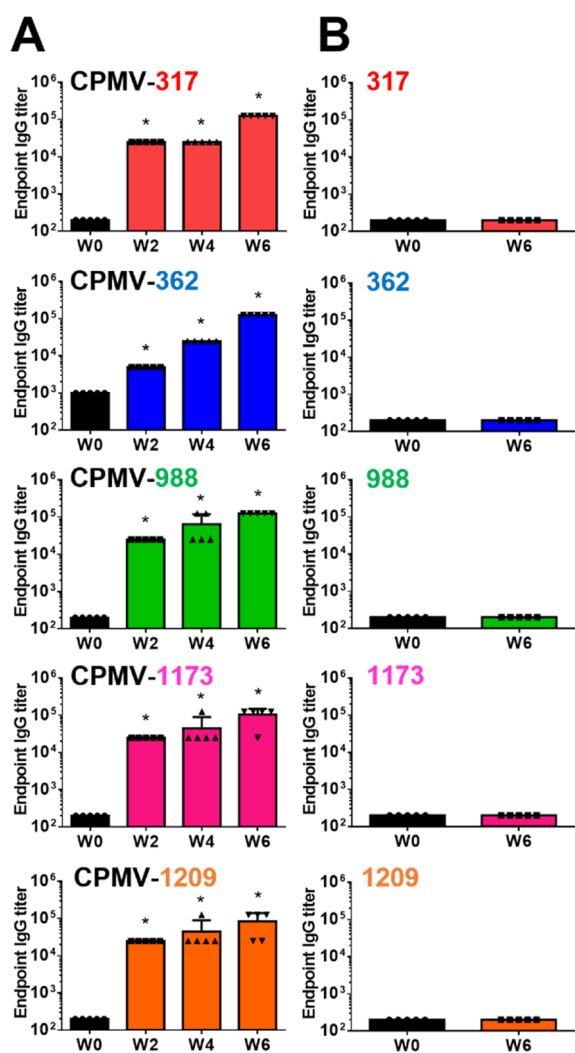
A

B

Figure 4. Binding of IgG to the SARS-CoV-2 S protein as determined by ELISA (*n* = 5 mice per group). (A) Endpoint IgG titers from animals vaccinated with red = CPMV-317, green = CPMV-988, pink = CPMV-1173, yellow = CPMV-1209, or blue = CPMV-362, at various times in weeks (W0−W10) after the first immunization (W0 corresponds to plasma collected prior to the first immunization). (B) Endpoint IgG titers from animals vaccinated with free peptides (color code identical to panel (A)). Statistical significance: *p < 0.0001 vs W0.

lymph nodes. The distribution of CPMV-Cy5 predominantly within the T-cell-rich zone was more evident in the cervical and inguinal lymph nodes, but the CPMV-Cy5 signal in all lymph nodes was similar. Finally, on day 28, the CPMV-Cy5 signal was not detected in the axillary lymph nodes, but a residual signal remained in the cervical lymph nodes and a slightly stronger signal in the inguinal lymph nodes. These observations suggest that CPMV-Cy5 drains initially to the lymph nodes closest to the implant zone, in this case the cervical lymph nodes (Figure 7, day 7), followed by a broader distribution to all lymph nodes by day 14. Ultimately, the last VNPs from the implant drain to the closest (cervical) lymph nodes and therefore show a stronger signal than the farthest (inguinal) lymph nodes. This corresponds to the degradation profile of the implant, with ∼50% of the CPMV-Cy5 released by day 14 and almost all released by day 28 (Figure 6D).

■ DISCUSSION

Beta-coronaviruses share a small number of conserved B-cell and T-cell epitopes on the N and S proteins that suggest that it may be possible to develop pan-beta-coronavirus vaccines that protect not only against known species such as the SARS-CoV-2 but also new variants and even new species that could, if not tackled preemptively, lead to future pandemics.[32,33] The S protein is considered the most suitable vaccine target for coronaviruses because it is responsible for interactions with host-cell receptors and cell fusion and thus elicits neutralizing antibodies.[17] We therefore selected five B-cell epitopes,[24] two within or adjacent to the RBD on the S1 subunit and three within the heptad repeats that define the stalk region of S2, which promotes membrane fusion (Figure 1). Importantly, all but one of the epitopes showed 100% sequence identity between the SARS-CoV and SARS-CoV-2 and were previously found to be immunogenic or reactive to sera from convalescent SARS-CoV patients.[37−39] Each epitope was (separately) conjugated to CPMV particles to produce soluble vaccine candidates,[40] and we also prepared a pentavalent implant by mixing equimolar amounts of all five candidates with PLGA and PEG to form a slow-release formulation.[51−53]

The display of peptides on the surface of plant viruses has been widely used as a strategy to develop vaccines, either by direct conjugation to virus particles or by the genetic engineering of coat proteins, but it is important to ensure that the peptides are compatible with virus assembly to avoid particle dissolution or aggregation.[54] DLS, TEM, and SDS-PAGE were used to confirm the structural integrity of the particles and also to determine the degree of antigen incorporation (Figure 2). DLS and TEM confirmed that the particles were monodisperse both before and after conjugation, indicating that conjugation neither destabilized the particles (resulting in them breaking into individual coat protein subunits) nor caused them to aggregate and precipitate from solution. SDS-PAGE analysis showed that each VNP presented 46−52 peptides suggesting comparable bioconjugation of all five peptides using the SM-(PEG)$_4$ linker and highlighting the flexibility of the CPMV platform in accommodating peptides ranging from 8 to 22 amino acid residues and varying pIs of 3.7 to 11.8. (Table 1).

The five vaccine candidates were then injected into mice, and we found that plasma from the immunized animals was able to bind to the corresponding peptides *in vitro*, whereas plasma from animals injected with free peptides was not (Figure 3). These experiments confirmed that the CPMV vaccine candidates were able to induce significant antibody titers after priming and two boosts. Notably, some candidates elicited high antibody titers that remained consistent over the 2−10 week time frame (CPMV-362 and CPMV-988), whereas others elicited initially lower antibody titers that increased over time (CPMV-317, CPMV-1173, and CPMV-1209). This highlights the potency of the CPMV, which serves as an antigen display and delivery technology but also as a potent adjuvant that stimulates innate immune cells by signaling through the Toll-like receptors. We recently demonstrated that the CPMV signals through TLR-2, TLR-4, and TLR-7.[55] The temporal variability of antibody titers is likely influenced by the intrinsic properties of peptides (Table 1; hydrophobicity, length, or relative positioning of certain residues) and could be evaluated in future studies. For example, it would be useful to establish the attributes of peptides that elicit high antibody
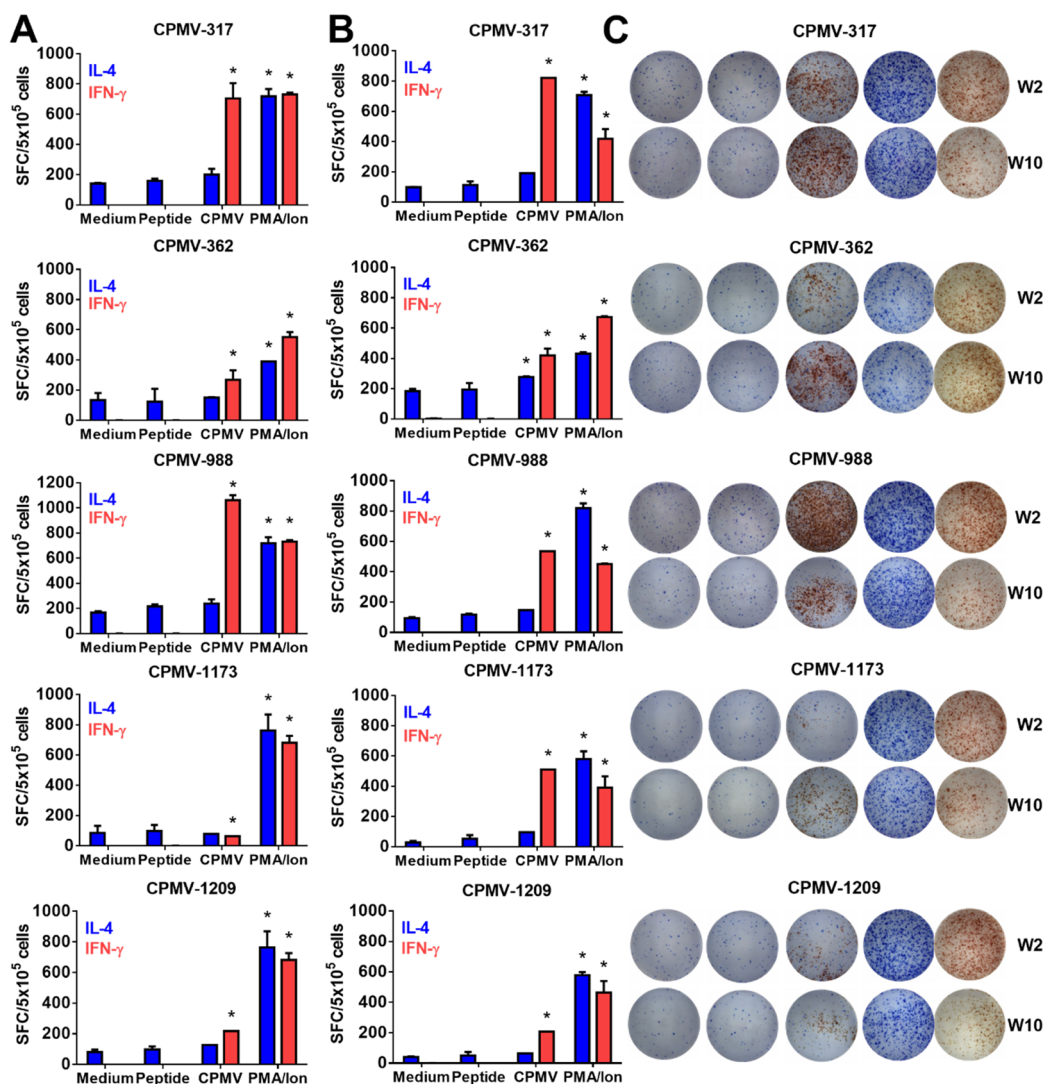
Figure 5. ELISpot assay with splenocytes from vaccinated mice. Isolated splenocytes (5×10^5 cells per well) from immunized mice ($n = 3$) were stimulated with the medium only (negative control), the matching free peptides (20 μg/mL), and the unmodified CPMV (10 μg/mL) or PMA (50 ng/mL) plus ionomycin (1 μg/mL) as a positive control. Cytokine-producing cells (IFN-γ or IL-4) were counted as spot-forming colonies (SFCs) from (A) week 2 (W2) or (B) W10 after the first immunization. (C) Representative images of blue (IL-4) and red (IFN-γ) spots formed by stimulated splenocytes from W2 or W10 after the first immunization. Statistical significance: *$p < 0.001$ vs the normal medium.

titers after a single dose when displayed on the CPMV and whether the administration of single doses of CPMV-362 and CPMV-988 would achieve lasting high antibody titers similar to those obtained after the prime-boost schedule. Likewise, the five vaccine candidates also differed in terms of the immune response based on the type of antibody produced. Interestingly, candidate CPMV-362 showed an immediate Th2-biased response, whereas all other candidates showed an initial Th1-biased response that switched to a Th2-biased response after 2 weeks (CPMV-317) or 6 weeks (all others). VNP-based vaccine platforms displaying multimeric self-epitopes or heterologous epitopes (target vaccine antigen) on the surface promote cross-linking of B-cell receptors (BCRs) that could prime B cells to induce the production of antibodies even without the help of CD4$^+$ T cells.[56,57] The CPMV, like other sub-200 nm nanoparticles, can diffuse and drain to lymph nodes without presentation on APCs, reaching zones rich in T and B cells in the lymph node periphery.[56,57] Early IgG2a (Th1-biased) responses may reflect fast and direct priming interactions between the CPMV vaccine candidates and B cells

in the lymph node, whereas later IgG1 (Th2-biased) responses after two boosts may favor APC presentation. Accordingly, although the CPMV was thought to be a clear Th1 adjuvant for peptide vaccines,[50,58] every new peptide/epitope must be tested on a case-by-case basis.

An early Th1 response was observed based on antibody isotypes, but the T-cell response did not mirror this response. We expected to see the production of IFN-γ, a signature cytokine for the Th1 profile, after coculturing the splenocytes from vaccinated mice with the same antigens used for the CPMV vaccines. The peptide alone may not be enough to stimulate the release of IFN-γ from T cells during the stimulation of splenocytes from vaccinated animals *in vitro* (Figure 5), or the Th1-biased isotype may reflect a direct priming interaction between the CPMV vaccine candidates and B cells, without the input of T cells to control isotype switching. These observations should be investigated in more detail in the future.

ELISAs confirmed that all five vaccines generated high titers of antibodies that bound to the corresponding peptides and to

Table 2. Neutralization Assay Data for Plasma Samples Taken from Mice Injected with the Five CPMV Vaccine Candidates[a]

plasma sample	assay name[b]	SARS-CoV[c]				SARS-CoV-2[d]		
		EC_{50}	CC_{50}	SI_{50}	neu. titer	EC_{50}	CC_{50}	SI_{50}
CPMV-317	visual	44	>250	5.7	160	>63	>63	0
	neutral red	41	>250	6.1	160	>63	>63	0
CPMV-362	visual	60	>250	4.2	80	>63	>63	0
	neutral red	51	>250	4.9	80	>63	>63	0
CPMV-988	visual	22	>250	**11**	**320**	>63	>63	0
	neutral red	22	>250	**11**	**320**	>63	>63	0
CPMV-1173	visual	22	>250	**11**	**320**	>63	>63	0
	neutral red	23	>250	**11**	**320**	>63	>63	0
CPMV-1209	visual	14	>250	**18**	**320**	>63	>63	0
	neutral red	16	>250	**16**	**320**	>63	>63	0
CPMV	visual	>250	>250	0	40	>63	>63	0
	neutral red	>250	>250	0	40	>63	>63	0

[a]EC_{50} = concentration (μg/mL) that reduces viral replication by 50%; CC_{50} = concentration (μg/mL) that reduces cell viability by 50%; SI_{50} = CC_{50}/EC_{50}; SI_{50} values >10 are considered as evidence of neutralizing activity. Neu. titer = viral neutralization titer at EC_{50}. Bold values represent the vaccine candidates considered as neutralizing. [b]Each assay was performed to test the cytopathic effect. [c]We used a range of concentrations of eight two-fold serial dilutions (250 to 1.9 μg/mL or dilution 1:40–1:5120). [d]We used a range of concentrations of eight two-fold serial dilutions (63 to 0.5 μg/mL or dilution 1:16–1:2048).

the recombinant SARS-CoV-2 S protein (Figure 4). However, *in* vitro neutralization assays against the SARS-CoV and SARS-CoV-2 showed that plasma samples from only three candidates, namely, CPMV-988, CPMV-1173, and CPMV-1209, were able to neutralize the SARS-CoV. Nevertheless, none of the candidates were able to neutralize the SARS-CoV-2 (Table 2). Possible explanations include the inaccessibility of corresponding epitopes on the S protein to the antibodies due to the conformation of the protein or the presence of post-translational modifications such as *N*-linked glycans or the inability of antibodies binding these epitopes to block interactions with hACE-2 or cause conformational changes that prevent receptor interactions.[59]

The inability of the CPMV-317 and CPMV-362 candidates to neutralize either virus may reflect the unique properties of the displayed peptides: the small size of peptide 317 (eight residues) and/or the high pI of both peptides (9.5 and 11.8, respectively) may interfere with their ability to fold properly when displayed on the CPMV particle, thus eliciting antibodies that lack neutralizing efficacy. Notably, only CPMV-317 and CPMV-362 elicited an IgG1-predominant response, and these were also the only two candidates that did not neutralize the SARS-CoV. Interestingly, although the other epitopes 988, 1173, and 1209 show 100% sequence identity in the SARS-CoV and SARS-CoV-2 S proteins, the antibodies elicited by the CPMV-based vaccines were only able to neutralize the SARS-CoV. It is possible that the epitopes fold differently in the two viruses due to differences in the flanking residues that alter the overall conformation of the S protein.[60] However, a more likely explanation is the difference in glycosylation between the two viruses. There are 22 *N*-linked glycan sites on the SARS-CoV-2 S protein compared to 23 on the SARS-CoV, with 18 of the sites common to both viruses, and the glycan shield density is lower in the SARS-CoV than SARS-CoV-2 and MERS.[61,62] The epitopes used in CPMV-1173 (KNHTSPDVDLGDISGI**N**) and CPMV-1209 (EIDRLNE-VAKNL**N**ESLIDLQEL) both contain a conserved glycosylation site (bold), representing positions 1155 and 1176 in the SARS-CoV S protein and positions 1173 and 1194 in the SARS-CoV-2 S protein. The selective *in vitro* neutralization of the SARS-CoV but not the SARS-CoV-2, at least in the case of

CPMV-1173 and CPMV-1209, may therefore reflect the different glycan shield density of each virus. However, it is unclear how this phenomenon affects CPMV-998, which does not contain a conserved glycosylation site and warrants further studies.

The COVID-19 pandemic highlights the need for innovation in vaccine design but also the need for more effective vaccine delivery strategies. The roll-out of mass vaccinations was burdened by the requirement of storage at ultra-low temperatures, delivery via injection thus requiring medical staff, and the requirement of a prime-boost vaccination schedule. Plant virus nanotechnologies hold potential to overcome the cold chain because these materials are stable under various environmental conditions. Toward overcoming the need for repeated injections, we evaluated the efficacy of a sustained release vaccine implant incorporating all five candidate vaccines. The five CPMV-based vaccine candidates were formulated as a pentavalent implant by hot-melt extrusion with PLGA and PEG8000.[44,51−53] Imaging studies revealed sustained release of the CPMV *in vivo* and trafficking of the CPMV to B- and T-cell-rich regions of the draining lymph nodes. Meanwhile, antibody titers against the CPMV carrier were 32-fold lower from the implant CPMV vs soluble injected CPMV vaccines (1:6400 vs 1:204,800, respectively; Figure S4). We found that the IgG titers against the target epitopes produced using the CPMV/PLGA implants releasing the pentavalent vaccine candidates were not as high as those induced by the corresponding soluble vaccines (Figure 5 for the implant vs Figure 3 for soluble vaccine candidates). The formulation process, which involves freezing, lyophilization, and heat extrusion, could be the underlying factor and influence the immunogenicity of the particles. DLS and TEM data were consistent with the intact CPMV being released from the polymer blends (Figure S3); however, the lyophilization step resulted in loss of the RNA cargo (Figure S2), which is consistent with our previous findings.[63] CPMV genomic RNA has been identified as a TLR-7 agonist, and its absence during antigen processing can mitigate the self-adjuvant properties of CPMV vaccines.[55] The difference of the antibody titers of CPMV implants compared to prime-boost formulations requires further analysis and may reflect a
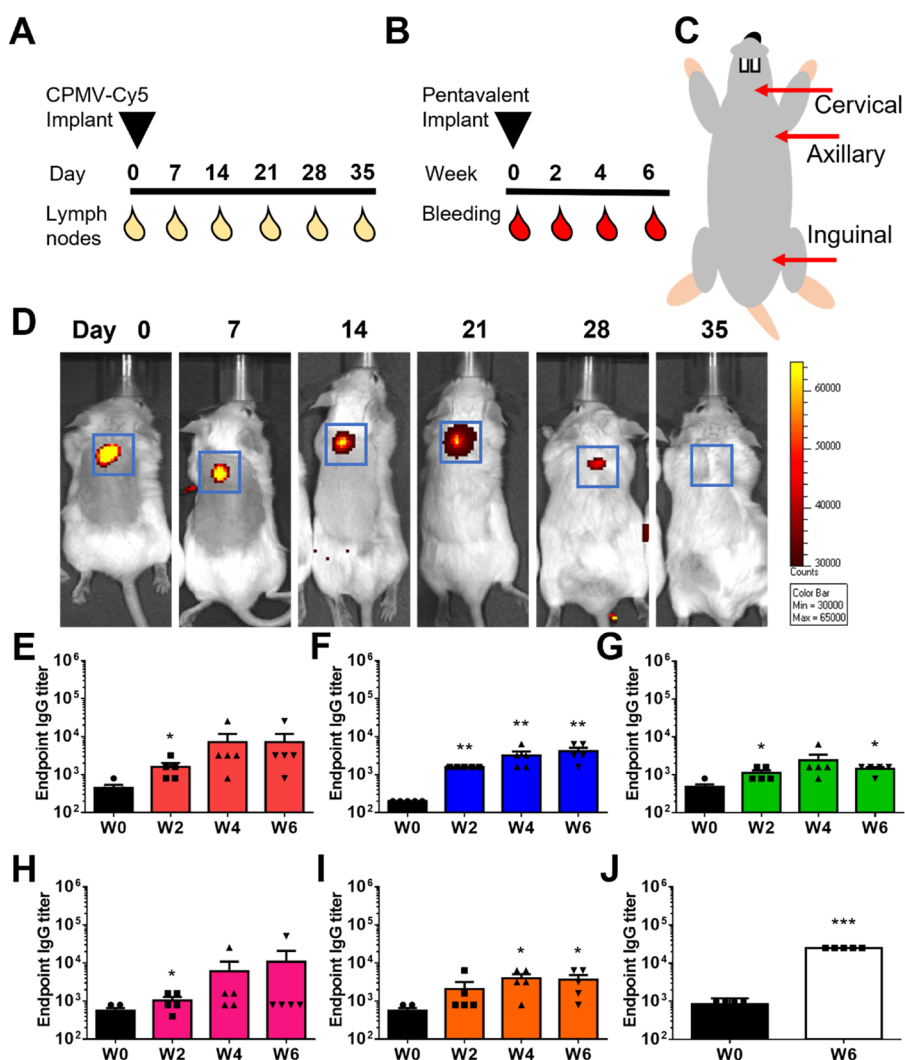
Figure 6. *In vivo* release of CPMV-Cy5 and the immunogenicity of pentavalent CPMV implants. (A) Administration schedule of CPMV-Cy5 implants and lymph node (LN) collection on different days ($n = 12$; $n = 2$ animals per day were euthanized for LN collection). (B) Administration schedule of pentavalent CPMV implants (CPMV-317, CPMV-362, CPMV-988, CPMV-1173, and CPMV-1209), $n = 5$. Three hundred micrograms of each CPMV vaccine per implant was used; this pentavalent implant dose is equivalent to a prime-boost-boost of 100 μg per dose for individual soluble vaccines. (C) Ventral view of the mouse, showing localization of the different LNs collected (two LNs collected per site). (D) *In vivo* fluorescence images of mice implanted (blue squares) with CPMV-Cy5, showing the Cy5 channel at different time points. (E−I) ELISA showing endpoint IgG titers (W0−W6) against peptides 317, 362, 988, 1173, and 1209. (J) ELISA showing endpoint IgG titers (W0 and W6) against the SARS-CoV-2 S protein. Statistical significance: *$p < 0.05$; **$p < 0.01$; ***$p < 0.0001$ vs week W0.

combination of RNA loss or other structural changes that influence subsequent interactions with (and activation of) innate immune cells. Future work will explore the addition of cryoprotectants before or during the lyophilization step to maintain the RNA cargo or addition of other TLR agonists as adjuvants. Furthermore, it cannot be ruled out that conformational changes of the epitope or the carrier impact vaccine efficacy. In previous work with VLPs from a bacteriophage presenting the human papilloma virus or cardiovascular disease-related epitopes, we reported matched efficacy of the implant vs soluble vaccine.[52,53] Another difference between the soluble prime-boost and slow-release implant is of course the dosing: 2 bolus doses vs sustained slower doses delivered by the implant. More research is needed to identify whether changes in antibody titers are based on the carrier or epitope properties post hot-melt extrusion or the delivery process itself.

■ CONCLUSIONS

We screened five B-cell epitopes originally identified in the convalescent sera from recovered SARS patients by displaying them on the surface of the CPMV. Three of these epitopes (peptides 988, 1173, and 1209) were found to be suitable for vaccine design. Immunization of mice using soluble formulation in a prime-boost-boost strategy elicited high antibody titers that neutralized the SARS-CoV *in vitro*. The neutralizing vaccine candidates (CPMV-988, CPMV-1173, and CPMV-1209) showed an early Th1-biased antibody profile (2−4 weeks) transitioning to a slightly Th2-biased profile after 6 weeks, just after the second boost. A pentavalent vaccine comprising all five peptides displayed on the CPMV was administered as a slow-release implant, and antibody titers were generated not as high as those elicited by the soluble formulation and maintained the specificity against the S protein. Sequence analysis revealed that the three epitopes (-988, -1173, and -1209) were 100% identical in the SARS-
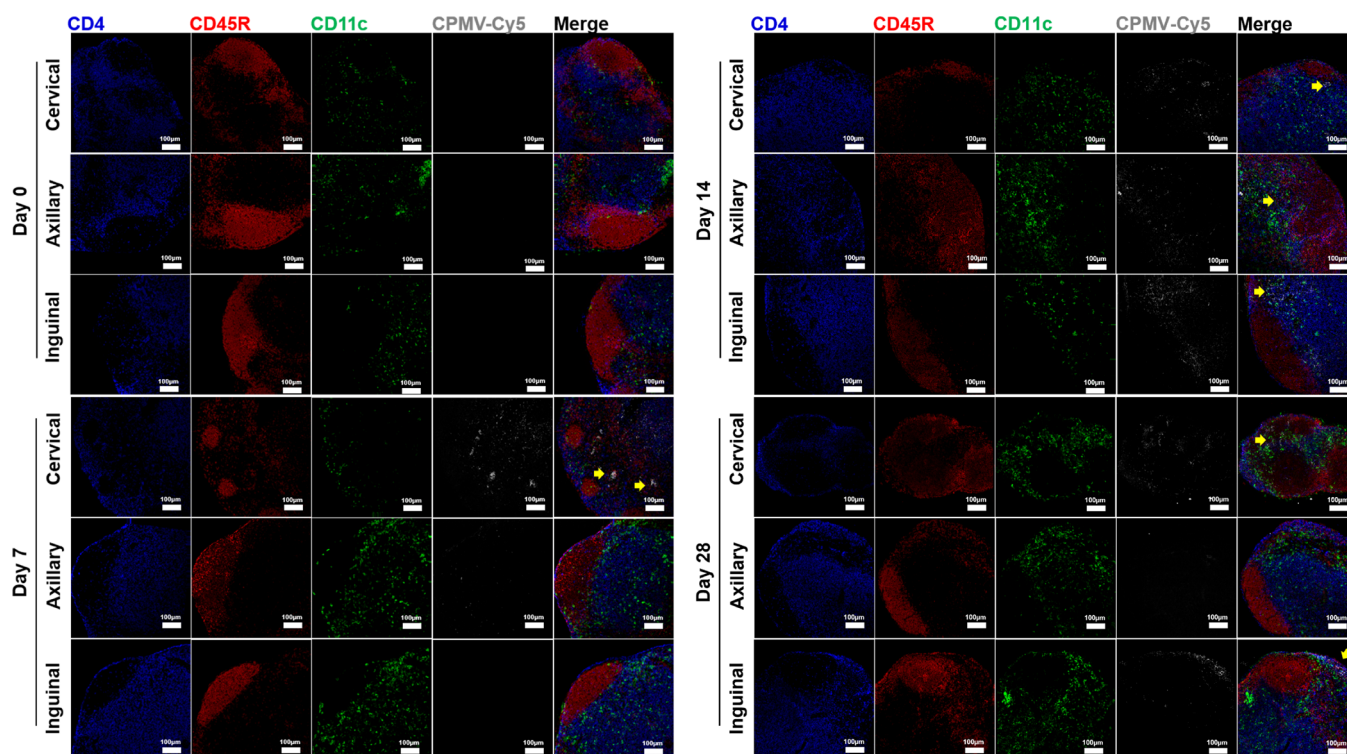
Figure 7. Immunofluorescence staining of T cells (CD4, blue), B cells (CD45R, red), dendritic cells (CD11c, green), and the CPMV (CPMV-Cy5, gray) and merged images of lymph nodes (cervical, axillary, and inguinal) at different time points after the administration of implants. Scale bar = 100 μm. Yellow arrows indicate the accumulation of CPMV-Cy5.

CoV and SARS-CoV-2, but none of the vaccine candidates were able to neutralize the SARS-CoV-2 suggesting differences in the structural context perhaps caused by conformational changes or the presence of N-linked glycans. Plant virus nanotechnologies offer high thermal stability, thus overcoming the need for cold chain storage and distribution. The technology presented here therefore offers a highly versatile vaccination platform that can be pivoted toward other diseases and applications that are not limited to infectious diseases.

■ METHODS

CPMV Propagation. VNPs based on the CPMV were propagated and purified as previously described.[64] Purified VNPs were stored in 0.1 M potassium phosphate (KP) buffer (pH 7.0) at 4 °C. VNP concentrations were determined by UV spectroscopy at 260 nm using the molar extinction coefficient ε_{CPMV} = 8.1 mL mg^{-1} cm^{-1}.

Antigen Characterization *In Silico*. We selected five B-cell epitopes[24] from the SARS-CoV-2 S protein (accession no. YP_009724390.1) as follows: 317 = KGIYQTSN, 362 = ATRFASVYAWNRKRISN, 988 = AISSVLNDILSRLDKVE, 1173 = KNHTSPDVDLGDISGIN, and 1209 = EIDRLNE-VAKNLNESLIDLQEL (Figure 1). We used an online peptide calculator (https://pepcalc.com/) to predict the molecular weights and isoelectric points. We determined the sequence identity compared to the SARS-CoV S protein (accession no. YP_009825051.1) using protein BLAST (https://blast.ncbi. nlm.nih.gov/).

Synthesis and Formulation of CPMV Vaccine Candidates. The five B-cell epitopes appended with an N-terminal cysteine residue a and triple glycine (GGG) linker were purchased from GenScript, with the following peptide sequences: 317 = C-GGG-KGIYQTSN, 362 = C-GGG-

ATRFASVYAWNRKRISN, 988 = C-GGG-AISSVLN-DILSRLDKVE, 1173 = C-GGG-KNHTSPDVDLGDISGIN, and 1209 = C-GGG-EIDRLNEVAKNLNESLIDLQEL. Using our two-step protocol,[65] each peptide epitope was conjugated to the CPMV capsid via the heterobifunctional N-hydrox-ysuccinimide (NHS)-PEG$_4$-maleimide linker SM-PEG$_4$ (Thermo Fisher Scientific) targeting the surface-exposed lysine residues. Briefly, wild-type CPMV particles (2 mg/mL in KP buffer) were reacted with a 3000-fold molar excess of the SM-PEG$_4$ linker at room temperature for 2 h followed by a 6000-fold molar excess of each peptide overnight. The resulting vaccine candidates CPMV-317, CPMV-362, CPMV-988, CPMV-1173, and CPMV-1209 were purified using Amicon spin columns with a cutoff of 100 kDa (Sigma-Aldrich), resuspended in sterile KP buffer, and stored at 4 °C.

Characterization of CPMV Vaccine Candidates. To verify peptide conjugation, 10 μg amounts of the unmodified CPMV and purified CPMV vaccine candidates (CPMV-317, CPMV-362, CPMV-988, CPMV-1173, and CPMV-1209) were compared by sodium dodecyl sulfate polyacrylamide gel electrophoresis (SDS-PAGE) under reducing conditions on NuPAGE 4−12% Bis-Tris protein gels (Thermo Fisher Scientific) and stained with GelCode Blue Safe (Thermo Fisher Scientific). Gel images were acquired using the ProteinSimple FluorChem R imaging system, and lane density analysis with ImageJ 1.44o (http://imagej.nih.gov/ij) was used to determine the number of peptides conjugated per VNP. Particle integrity was confirmed by transmission electron microscopy (TEM) using a Tecnai Spirit G2 Bio TWIN (FEI Technologies) following 2% (w/v) uranyl acetate staining. Particle size was measured by dynamic light scattering (DLS) on a Zetasizer Nano (Malvern Instruments) at 25 °C in plastic disposable cuvettes.

Preparation of CPMV Implants by Hot-Melt Extrusion. Poly(lactic-*co*-glycolic acid) (PLGA) implants were prepared as previously described using our desktop melt-processing system.[45,51−53] Briefly, PLGA powder with a 50:50 L/G ratio and a molecular weight of 10−15 kDa (Akina) was passed through a 45-mesh sieve (Sigma-Aldrich) for implant formulation. Lyophilized CPMV-317, CPMV-362 CPMV-988, CPMV-1173, and CPMV-1209 were mixed in equal amounts and then combined with PLGA and PEG8000 (Fisher Scientific) in the following ratio: 75% PLGA, 10% VNPs, and 15% PEG8000 (wt %). The components were mixed by vortexing, loaded into the hot melt-processing system, and heated to 70 °C for 90 s. Implants were extruded at a pressure of 10 psi applied to the piston. Implants were dried and stored with desiccants until use. CPMV-Cy5 implants were processed in the same manner.

Immunization. All animal experiments were carried out in compliance with guidelines from the UC San Diego Institutional Animal Care and Use Committee. Eight-week-old male BALB/c mice (Jackson Laboratory) were kept under standard conditions with food and water provided *ad libitum*. Five mice were assigned per experimental group. For the subcutaneous injection of liquid formulations, each CPMV vaccine candidate was concentrated at 1 mg/mL in phosphate-buffered saline (PBS; 137 mM NaCl, 2.7 mM KCl, 10 mM Na_2HPO_4, and 1.8 mM KH_2PO_4, pH 7.4), and 100 μL was injected three times (100 μg/dose) at 2-week intervals (prime + two boosts). For the implant, a single dose containing 300 μg of each vaccine candidate (mimicking the 100 μg per dose subcutaneous injection) was administered using an 18G needle (BD Sciences) behind the neck. We also administered 5 μg per dose of the free peptides (equivalent to peptides present in a 100 μg dose of the CPMV-peptide vaccine) to a control group. Retro-orbital blood was collected in lithium/heparin-treated tubes (Thomas Scientific) just before injection or implantation (week 0) and then at weeks 2, 4, 6, and 10. Plasma was collected by centrifugation at 2000g for 10 min at room temperature and was stored at −80 °C.

IgG Titers against Peptides and the S Protein. Endpoint total IgG titers against each peptide epitope were determined by enzyme-linked immunosorbent assay (ELISA) in 96-well maleimide-activated plates (Thermo Fisher Scientific). Briefly, the plates were coated with 100 μL per well of each peptide (25 μg/mL in coating buffer: 0.1 M sodium phosphate, 0.15 M sodium chloride, and 10 mM EDTA, pH 7.2) overnight at 4 °C. After three washes with 200 μL per well of PBS + 0.5% Tween-20 (PBST), the plates were blocked for 1 h at room temperature using 200 μL per well of 10 μg/mL L-cysteine (Sigma-Aldrich). After washing again as above, plasma from immunized animals was prepared as two-fold serial dilutions in coating buffer and added to the plates. After incubation for 1 h at room temperature and another washing step, binding was detected using a horseradish peroxidase (HRP)-labeled goat antimouse IgG secondary antibody (Thermo Fisher Scientific) diluted 1:5000 in PBST (100 μL per well) for 1 h at room temperature. After a final washing step, we added 100 μL per well of a 1-Step Ultra TMB substrate (Thermo Fisher Scientific) and incubated it for 10 min before stopping the reaction with 100 μL per well of 2 M H_2SO_4.

The IgG titer against the SARS-CoV-2 S-protein was determined as described above but using 96-well nickel-activated plates (Thermo Fisher Scientific) coated with 200 ng of the His-tagged S protein per well (GenScript). Plasma samples were diluted five-fold in PBS, and the same secondary antibody dilution and substrate were used to develop the assay as described above. The absorbance was read at 450 nm on a Tecan microplate reader. The endpoint antibody titers were defined as the reciprocal serum dilution at which the absorbance exceeded twice the background value (blank wells without plasma samples).

Antibody Isotyping. The ELISA method set out above was adapted for antibody isotyping by testing samples from weeks 2, 4, 6, and 10 (diluted 1:1000 in coating buffer) with the following HRP-labeled secondary antibodies (Abcam) and dilutions: goat antimouse IgG1 (1:5000), IgG2a (1:1000), IgG2b (1:5000), IgG2c (1:5000), IgG3 (1:5000), IgM (1:5000), and IgE (1:1000). The IgG1/IgG2a ratio was reported for each group, and a ratio higher than 1 was considered to indicate a Th2 response.

ELISpot Assays. Briefly, 96-well ELISpot plates (Cellular Technology) were coated with a 1:166 dilution of the antimouse interferon gamma (IFN-γ) and interleukin-4 (IL-4) capture antibodies overnight at 4 °C. Splenocyte suspensions collected from three mice, 2 or 10 weeks post-immunization with each CPMV vaccine candidate, were added to the plates (5 × 10^5 cells per well) following stimulation with 100 μL of the medium alone (negative control), free peptide epitopes (20 μg/mL), the unmodified CPMV (10 μg/mL), or 50 ng/mL phorbol 12-myristate 13-acetate (PMA) and 1 μg/mL ionomycin (Sigma-Aldrich) (positive control) at 37 °C and 5% CO_2 for 24 h. The plates were washed with PBST and then incubated with a 1:1000 dilution of FITC-labeled antimouse IFN-γ and a 1:666 dilution of biotin-labeled antimouse IL-4 antibodies at room temperature for 2 h. The plates were then washed with PBST and incubated at room temperature for 1 h with streptavidin-alkaline phosphatase (AP) and anti-FITC-HRP secondary antibodies (diluted 1:1000). Plates were washed with PBST and distilled water, then incubated with the AP substrate for 15 min at room temperature, washed with distilled water, and incubated with the HRP substrate for 10 min at room temperature. Plates were then rinsed with water and air-dried at room temperature overnight. Colored spots were quantified using an S6 ENTRY Analyzer (Immunospot). The splenocytes from each animal were tested in triplicate for each stimulant.

Neutralization Assays. The primary cytopathic effect assay[66] was carried out via the Preclinical Services offered by The National Institute of Allergy and Infectious Diseases (NIAID). The SARS-CoV strain Urbani and the SARS-CoV-2 strain USA_WA1/2020 were used to test neutralizing plasma. Briefly, confluent or near-confluent monolayers of Vero 76 cells were prepared in 96-well disposable microplates the day before testing. Cells were maintained in MEM (Sigma-Aldrich) supplemented with 5% fetal bovine serum (FBS) and were tested in the same medium with the FBS concentration reduced to 2% and supplemented with 50 μg/mL gentamicin. The pooled plasma samples (week 6 post-immunization) representing each CPMV vaccine candidate and the unmodified CPMV as a negative control were prepared as 10-fold serial dilutions. Five microwells were used per dilution: three for infected cultures and two for uninfected toxicity cultures. Controls consisted of six wells that were infected and not treated (virus controls) and six that were untreated and uninfected (cell controls) on every plate. Plasma samples were mixed with the virus (1:1 ratio) and incubated for 1 h at 37 °C.

The growth medium was then removed from the cells, and the plasma/virus mixture was applied (0.1 mL per well). For the virus infection controls, the virus was added typically at ~60 $CCID_{50}$ (50% cell culture infectious dose) in 0.1 mL of the medium. A medium without the virus was added to the toxicity control and cell control wells. Plates were incubated at 37 °C in a 5% CO_2 incubator until a cytopathic effect CPE > 80% was observed in the virus control wells. The plates were then stained with 0.011% neutral red for ~2 h at 37 °C in a 5% CO_2 incubator. The neutral red medium was removed, and the cells were rinsed with PBS to remove the residual dye. PBS was completely removed, and the incorporated neutral red was eluted with 50% Sorensen's citrate buffer/50% ethanol for at least 30 min. The dye content in each well, proportional to the number of living cells, was quantified by spectrophotometry at 540 nm. The dye content in each set of wells was converted to a percentage of the dye present in untreated control wells and normalized against the virus control. The 50% effective concentration (EC_{50}, virus inhibition) and 50% cytotoxic concentration (CC_{50}, cell inhibition) were calculated by regression analysis. The CC_{50}/EC_{50} quotient was used to calculate the selectivity index (SI), and plasma samples with SI $\geq$ 10 were considered as neutralizing.

Immunofluorescence Imaging of Lymph Nodes. Cy5-labeled CPMV nanoparticles were prepared for imaging studies. Fluorescent CPMV-Cy5 particles were synthesized by conjugating N-hydroxysuccinimide-activated esters of sulfo-Cy5 (NHS-sulfo-Cy5, Lumiprobe) to the CPMV capsid via the surface-exposed lysine residues. Briefly, a 1500 molar excess of NHS-sulfo-Cy5 was reacted overnight with the CPMV in 0.1 M KP buffer (pH 7.4) plus 10% (v/v) DMSO and a protein concentration of 2 mg/mL. Following the reaction, Cy5-conjugated particles were purified from the excess unreacted dye by ultracentrifugation (112,000g, 1 h). The pellet was then resuspended in 0.1 M KP buffer. The CPMV concentration and the number of dye molecules per capsid were determined by UV/vis spectrophotometry using the CPMV extinction coefficient (ε_{CPMV}) = 8.1 mL mg^{-1} cm^{-1} at 260 nm and the NHS-sulfo-Cy5 specific molar extinction coefficient ($\varepsilon_{sulfo\text{-}Cy5}$) = 27,1000 L mol^{-1} cm^{-1} at 647 nm. CPMV-Cy5 implants were prepared as described above and introduced subcutaneously via an 18G needle by pushing the implant out of the needle using a sterilized stainless-steel wire (0.51 mm diameter). Fluorescence images were acquired on an IVIS 200 imaging system at different time points and were analyzed using Living Image v3.0. To determine the fate of VNPs in the implant, cervical, axillary, and inguinal lymph nodes were collected from the mice in 10% formalin-buffered solution (Sigma-Aldrich) on days 0, 7, 14, 21, 28, and 35 after CPMV-Cy5 implant administration. Two mice were euthanized on each day. The lymph nodes were embedded in paraffin, and tissue sections were stained for the cell surface markers CD11c (LS Bio, 1:25), CD45R (Abcam, 1:50), and CD4 (Abcam, 1:100). A donkey antirabbit IgG secondary antibody conjugated to AlexaFluor 488 (Invitrogen, 1:500) was used to detect primary antibody binding. The sections were imaged on a Nikon A1R confocal microscope with an X20, 0.75 numerical aperture dry objective. Portions from two lymph node sections were imaged for each cell marker, and the corresponding channels were superimposed by aligning the DAPI signal to form composite images using Nikon Analysis software.

Statistical Analysis. Data are presented as the mean ± SEM. Single comparisons based on an unpaired, two-tailed t-test were carried out using SPSS Statistics software or GraphPad Prism 6. Differences were considered significant at $p < 0.05$. The number of replicates is described for each experiment.

■ ASSOCIATED CONTENT

ⓈⅠ Supporting Information

The Supporting Information is available free of charge at https://pubs.acs.org/doi/10.1021/acsinfecdis.1c00410.

Ig isotype profile (Figure S1), characterization of CPMV-Cy5 (Figure S2) and CPMV released from PLGA implants (Figure S3), and IgG titers against CPMV comparing soluble vs implant administration (Figure S4) (PDF)

■ AUTHOR INFORMATION

Corresponding Author

Nicole F. Steinmetz − *Department of NanoEngineering, Center for Nano-ImmunoEngineering, Institute for Materials Discovery and Design, Department of Bioengineering, Department of Radiology, and Moores Cancer Center, University of California-San Diego, La Jolla, California 92039, United States;* ● orcid.org/0000-0002-0130-0481; Email: nsteinmetz@ucsd.edu

Authors

Oscar A. Ortega-Rivera − *Department of NanoEngineering and Center for Nano-ImmunoEngineering, University of California-San Diego, La Jolla, California 92039, United States;* ● orcid.org/0000-0002-0773-0677

Sourabh Shukla − *Department of NanoEngineering and Center for Nano-ImmunoEngineering, University of California-San Diego, La Jolla, California 92039, United States;* ● orcid.org/0000-0001-9751-5833

Matthew D. Shin − *Department of NanoEngineering and Center for Nano-ImmunoEngineering, University of California-San Diego, La Jolla, California 92039, United States*

Angela Chen − *Department of NanoEngineering and Center for Nano-ImmunoEngineering, University of California-San Diego, La Jolla, California 92039, United States*

Veronique Beiss − *Department of NanoEngineering and Center for Nano-ImmunoEngineering, University of California-San Diego, La Jolla, California 92039, United States*

Miguel A. Moreno-Gonzalez − *Department of NanoEngineering and Center for Nano-ImmunoEngineering, University of California-San Diego, La Jolla, California 92039, United States;* ● orcid.org/0000-0002-1601-9369

Yi Zheng − *Department of NanoEngineering and Center for Nano-ImmunoEngineering, University of California-San Diego, La Jolla, California 92039, United States*

Alex E. Clark − *Department of Medicine, University of California-San Diego, La Jolla, California 92039, United States*

Aaron F. Carlin − *Department of Medicine, University of California-San Diego, La Jolla, California 92039, United States;* ● orcid.org/0000-0002-1669-8066

Jonathan K. Pokorski − *Department of NanoEngineering, Center for Nano-ImmunoEngineering, and Institute for Materials Discovery and Design, University of California-San*

Diego, La Jolla, California 92039, United States;
orcid.org/0000-0001-5869-6942

Complete contact information is available at:
https://pubs.acs.org/10.1021/acsinfecdis.1c00410

Notes

■ ACKNOWLEDGMENTS

■ REFERENCES

(1) Almeida, J. D.; Berry, D. M.; Cunningham, C. H.; Hamre, D.; Hofstad, M. S.; Mallucci, L.; McIntosh, K.; Tyrrell, D. A. Virology: Coronaviruses. *Nature* 1968, 220, 650.

(2) Wertheim, J. O.; Chu, D. K. W.; Peiris, J. S. M.; Pond, S. L. K.; Poon, L. L. M. A case for the ancient origin of coronaviruses. *J. Virol.* 2013, 87, 7039−7045.

(3) Jevšnik, M.; Uršič, T.; Žigon, N.; Lusa, L.; Krivec, U.; Petrovec, M. Coronavirus infections in hospitalized pediatric patients with acute respiratory tract disease. *BMC Infect. Dis.* 2012, 12, 365.

(4) Chan-Yeung, M.; Xu, R. H. SARS: epidemiology. *Respirology* 2003, 8, S9−S14.

(5) Zumla, A.; Hui, D. S.; Perlman, S. Middle East respiratory syndrome. *Lancet* 2015, 386, 995−1007.

(6) Wang, C.; Horby, P. W.; Hayden, F. G.; Gao, G. F. A novel coronavirus outbreak of global health concern. *Lancet* 2020, 395, 470−473.

(7) *Johns Hopkins University of Medicine (2021) COVID-19 Dashboard*. Online resource (https://coronavirus.jhu.edu/map.html). Accessed 22/6/2021.

(8) *London School of Hygiene & Tropical Medicine (2021) COVID-19 vaccine tracker*. Online resource (https://vac-lshtm.shinyapps.io/ncov_vaccine_landscape/). Accessed 22/6/2021.

(9) Capell, T.; Twyman, R. M.; Armario-Najera, V.; Ma, J. K.-C.; Schillberg, S.; Christou, P. Potential applications of plant biotechnology against SARS-CoV-2. *Trends Plant Sci.* 2020, 25, 635−643.

(10) Lu, G.; Wang, Q.; Gao, G. F. Bat-to-human: spike features determining 'host jump' of coronaviruses SARS-CoV, MERS-CoV, and beyond. *Trends Microbiol.* 2015, 23, 468−478.

(11) Li, F.; Li, W.; Farzan, M.; Harrison, S. C. Structure of SARS coronavirus spike receptor-binding domain complexed with receptor. *Science* 2005, 309, 1864−1868.

(12) Lu, G.; Hu, Y.; Wang, Q.; Qi, J.; Gao, F.; Li, Y.; Zhang, Y.; Zhang, W.; Yuan, Y.; Bao, J.; Zhang, B.; Shi, Y.; Yan, J.; Gao, G. F. Molecular basis of binding between novel human coronavirus MERS-CoV and its receptor CD26. *Nature* 2013, 500, 227−231.

(13) Yan, R.; Zhang, Y.; Li, Y.; Xia, L.; Guo, Y.; Zhou, Q. Structural basis for the recognition of SARS-CoV-2 by full-length human ACE2. *Science* 2020, 367, 1444−1448.

(14) Li, W.; Moore, M. J.; Vasilieva, N.; Sui, J.; Wong, S. K.; Berne, M. A.; Somasundaran, M.; Sullivan, J. L.; Luzuriaga, K.; Greenough, T. C.; Choe, H.; Farzan, M. Angiotensin-converting enzyme 2 is a functional receptor for the SARS coronavirus. *Nature* 2003, 426, 450−454.

(15) Hoffmann, M.; Kleine-Weber, H.; Schroeder, S.; Krüger, N.; Herrler, T.; Erichsen, S.; Schiergens, T. S.; Herrler, G.; Wu, N.-H.; Nitsche, A.; Müller, M. A.; Drosten, C.; Pöhlmann, S. SARS-CoV-2 cell entry depends on ACE2 and TMPRSS2 and is blocked by a clinically proven protease inhibitor. *Cell* 2020, 181, 271−280.e8.

(16) Raj, V. S.; Mou, H.; Smits, S. L.; Dekkers, D. H.; Müller, M. A.; Dijkman, R.; Muth, D.; Demmers, J. A.; Zaki, A.; Fouchier, R. A.; Thiel, V.; Drosten, C.; Rottier, P. J. M.; Osterhaus, A. D. M. E.; Bosch, B. J.; Haagmans, B. L. Dipeptidyl peptidase 4 is a functional receptor for the emerging human coronavirus-EMC. *Nature* 2013, 495, 251−254.

(17) Jiang, S.; Hillyer, C.; Du, L. Neutralizing antibodies against SARS-CoV-2 and other human coronaviruses. *Trends Immunol.* 2020, 41, 355−359.

(18) Su, S.; Du, L.; Jiang, S. Learning from the past: development of safe and effective COVID-19 vaccines. *Nat Rev Microbiol* 2021, 19, 211−219.

(19) Yang, J.; Wang, W.; Chen, Z.; Lu, S.; Yang, F.; Bi, Z.; Bao, L.; Mo, F.; Li, X.; Huang, Y.; Hong, W.; Yang, Y.; Zhao, Y.; Ye, F.; Lin, S.; Deng, W.; Chen, H.; Lei, H.; Zhang, Z.; Luo, M.; Gao, H.; Zheng, Y.; Gong, Y.; Jiang, X.; Xu, Y.; Lv, Q.; Li, D.; Wang, M.; Li, F.; Wang, S.; Wang, G.; Yu, P.; Qu, Y.; Yang, L.; Deng, H.; Tong, A.; Li, J.; Wang, Z.; Yang, J.; Shen, G.; Zhao, Z.; Li, Y.; Luo, J.; Liu, H.; Yu, W.; Yang, M.; Xu, J.; Wang, J.; Li, H.; Wang, H.; Kuang, D.; Lin, P.; Hu, Z.; Guo, W.; Cheng, W.; He, Y.; Song, X.; Chen, C.; Xue, Z.; Yao, S.; Chen, L.; Ma, X.; Chen, S.; Gou, M.; Huang, W.; Wang, Y.; Fan, C.; Tian, Z.; Shi, M.; Wang, F. S.; Dai, L.; Wu, M.; Li, G.; Wang, G.; Peng, Y.; Qian, Z.; Huang, C.; Lau, J. Y. N.; Yang, Z.; Wei, Y.; Cen, X.; Peng, X.; Qin, C.; Zhang, K.; Lu, G.; Wei, X. A vaccine targeting the RBD of the S protein of SARS-CoV-2 induces protective immunity. *Nature* 2020, 586, 572−577.

(20) Wang, N.; Shang, J.; Jiang, S.; Du, L. Subunit vaccines against emerging pathogenic human coronaviruses. *Front. Microbiol.* 2020, 11, 298.

(21) Dai, L.; Zheng, T.; Xu, K.; Han, Y.; Xu, L.; Huang, E.; An, Y.; Cheng, Y.; Li, S.; Liu, M.; Yang, M.; Li, Y.; Cheng, H.; Yuan, Y.; Zhang, W.; Ke, C.; Wong, G.; Qi, J.; Qin, C.; Yan, J.; Gao, G. F. A universal design of betacoronavirus vaccines against COVID-19, MERS, and SARS. *Cell* 2020, 182, 722−733.e11.

(22) Ward, B. J.; Gobeil, P.; Séguin, A.; Atkins, J.; Boulay, I.; Charbonneau, P.-Y.; Couture, M.; D'Aoust, M. A.; Dhaliwall, J.; Finkle, C.; Hager, K.; Mahmood, A.; Makarkov, A.; Cheng, M. P.; Pillet, S.; Schimke, P.; St-Martin, S.; Trépanier, S.; Landry, N. Phase 1 randomized trial of a plant-derived virus-like particle vaccine for COVID-19. *Nat. Med.* 2021, 27, 1071−1078.

(23) Hu, B.; Guo, H.; Zhou, P.; Shi, Z.-L. Characteristics of SARS-CoV-2 and COVID-19. *Nat. Rev. Microbiol.* 2021, 19, 141−154.

(24) Ahmed, S. F.; Quadeer, A. A.; McKay, M. R. Preliminary identification of potential vaccine targets for the COVID-19 coronavirus (SARS-CoV-2) based on SARS-CoV immunological studies. *Viruses* 2020, 12, 254.

(25) Shin, M. D.; Shukla, S.; Chung, Y. H.; Beiss, V.; Chan, S. K.; Ortega-Rivera, O. A.; Wirth, D. M.; Chen, A.; Sack, M.; Pokorski, J. K.; Steinmetz, N. F. COVID-19 vaccine development and a potential nanomaterial path forward. *Nat. Nanotechnol.* 2020, 15, 646−655.

(26) Zhu, Y.; Yu, D.; Han, Y.; Yan, H.; Chong, H.; Ren, L.; Wang, J.; Li, T.; He, Y. Cross-reactive neutralization of SARS-CoV-2 by serum antibodies from recovered SARS patients and immunized animals. *Sci. Adv.* 2020, 6, No. eabc9999.

(27) Zang, J.; Gu, C.; Zhou, B.; Zhang, C.; Yang, Y.; Xu, S.; Bai, L.; Zhang, R.; Deng, Q.; Yuan, Z.; Tang, H.; Qu, D.; Lavillette, D.; Xie, Y.; Zhang, X. Immunization with the receptor-binding domain of SARS-CoV-2 elicits antibodies cross-neutralizing SARS-CoV-2 and SARS-CoV without antibody-dependent enhancement. *Cell Discovery* 2020, 6, 61.

(28) Tai, W.; Zhang, X.; Drelich, A.; Shi, J.; Hsu, J. C.; Luchsinger, L.; Hillyer, C. D.; Tseng, C.-T. K.; Jiang, S.; Du, L. A novel receptor-

binding domain (RBD)-based mRNA vaccine against SARS-CoV-2. *Cell Res* **2020**, *30*, 932−935.

(29) Tai, W.; Zhang, X.; He, Y.; Jiang, S.; Du, L. Identification of SARS-CoV RBD-targeting monoclonal antibodies with cross-reactive or neutralizing activity against SARS-CoV-2. *Antiviral Res.* **2020**, *179*, 104820.

(30) Pinto, D.; Park, Y.-J.; Beltramello, M.; Walls, A. C.; Tortorici, M. A.; Bianchi, S.; Jaconi, S.; Culap, K.; Zatta, F.; De Marco, A.; Peter, A.; Guarino, B.; Spreafico, R.; Cameroni, E.; Case, J. B.; Chen, R. E.; Havenar-Daughton, C.; Snell, G.; Telenti, A.; Virgin, H. W.; Lanzavecchia, A.; Diamond, M. S.; Fink, K.; Veesler, D.; Corti, D. Cross-neutralization of SARS-CoV-2 by a human monoclonal SARS-CoV antibody. *Nature* **2020**, *583*, 290−295.

(31) Wec, A. Z.; Wrapp, D.; Herbert, A. S.; Maurer, D. P.; Haslwanter, D.; Sakharkar, M.; Jangra, R. K.; Dieterle, M. E.; Lilov, A.; Huang, D.; Tse, L. V.; Johnson, N. V.; Hsieh, C. L.; Wang, N.; Nett, J. H.; Champney, E.; Burnina, I.; Brown, M.; Lin, S.; Sinclair, M.; Johnson, C.; Pudi, S.; Bortz, R., III; Wirchnianski, A. S.; Laudermilch, E.; Florez, C.; Fels, J. M.; O'Brien, C. M.; Graham, B. S.; Nemazee, D.; Burton, D. R.; Baric, R. S.; Voss, J. E.; Chandran, K.; Dye, J. M.; McLellan, J. S.; Walker, L. M. Broad neutralization of SARS-related viruses by human monoclonal antibodies. *Science* **2020**, *369*, 731−736.

(32) Cao, M.; Su, X.; Jiang, S. Broad-spectrum anti-coronavirus vaccines and therapeutics to combat the current COVID-19 pandemic and future coronavirus disease outbreaks. *Stem Cell Rep.* **2021**, *16*, 398−411.

(33) Cohen, J. *Vaccines that can protect against many coronaviruses could prevent another pandemic*; Science online article, 2021 DOI: 10.1126/science.abi9939.

(34) Lucchese, G. Epitopes for a 2019-nCoV vaccine. *Cell Mol. Immunol.* **2020**, *17*, 539−540.

(35) Grifoni, A.; Sidney, J.; Zhang, Y.; Scheuermann, R. H.; Peters, B.; Sette, A. A sequence homology and bioinformatic approach can predict candidate targets for immune responses to SARS-CoV-2. *Cell Host Microbe* **2020**, *27*, 671−680.e2.

(36) Baruah, V.; Bose, S. Immunoinformatics-aided identification of T cell and B cell epitopes in the surface glycoprotein of 2019-nCoV. *J. Med. Virol.* **2020**, *92*, 495−500.

(37) Guo, J. P.; Petric, M.; Campbell, W.; McGeer, P. L. SARS corona virus peptides recognized by antibodies in the sera of convalescent cases. *Virology* **2004**, *324*, 251−256.

(38) He, Y.; Zhou, Y.; Wu, H.; Luo, B.; Chen, J.; Li, W.; Jiang, S. Identification of immunodominant sites on the spike protein of severe acute respiratory syndrome (SARS) coronavirus: implication for developing SARS diagnostics and vaccines. *J. Immunol.* **2004**, *173*, 4050−4057.

(39) Wang, Q.; Zhang, L.; Kuwahara, K.; Li, L.; Liu, Z.; Li, T.; Zhu, H.; Liu, J.; Xu, Y.; Xie, J.; Morioka, H.; Sakaguchi, N.; Qin, C.; Liu, G. Immunodominant SARS coronavirus epitopes in humans elicited both enhancing and neutralizing effects on infection in non-human primates. *ACS Infect.Dis.* **2016**, *2*, 361−376.

(40) Steinmetz, N. F.; Lin, T.; Lomonossoff, G. P.; Johnson, J. E. Structure-based engineering of an icosahedral virus for nanomedicine and nanotechnology. *Viruses Nanotechnol.* **2009**, *327*, 23−58.

(41) ClinicalTrials.gov . *Study of a recombinant coronavirus-like particle COVID-19 vaccine in adults*. Online resource (https://clinicaltrials.gov/ct2/show/NCT04636697). Accessed 22/6/2021.

(42) Lee, P. W.; Pokorski, J. K. Poly(lactic-co-glycolic acid) devices: production and applications for sustained protein delivery. *WIRES Nanomed. Nanobiotechnol.* **2018**, *10*, No. e1516.

(43) Lee, P. W.; Maia, J.; Pokorski, J. K. Milling solid proteins to enhance activity after melt-encapsulation. *Int. J. Pharm.* **2017**, *533*, 254−265.

(44) Lee, P. W.; Shukla, S.; Wallat, J. D.; Danda, C.; Maia, J.; Steinmetz, N. F.; Pokorski, J. K. Virus-like particle laden biodegradable implants prepared via melt processing. *ACS Nano* **2017**, *11*, 8777−8789.

(45) Lee, P. W.; Isarov, S. A.; Wallat, J. D.; Molugu, S. K.; Shukla, S.; Sun, J. E. P.; Zhang, J.; Zheng, Y.; Lucius Dougherty, M.; Konkolewicz, D.; Stewart, P. L.; Steinmetz, N. F.; Hore, M. J. A.; Pokorski, J. K. Polymer structure and conformation alter immune recognition of virus-like particle-polymer conjugates. *J. Am. Chem. Soc.* **2017**, *139*, 3312−3315.

(46) Lee, P. W.; Towslee, J. H.; Maia, J.; Pokorski, J. K. PEGylation to improve protein stability during melt processing. *Macromol. Biosci.* **2015**, *15*, 1332−1337.

(47) Coutard, B.; Valle, C.; de Lamballerie, X.; Canard, B.; Seidah, N. G.; Decroly, E. The spike glycoprotein of the new coronavirus 2019-NCoV contains a furin-like cleavage site absent in CoV of the same clade. *Antiviral Res.* **2020**, *176*, 104742.

(48) Guruprasad, L. Human SARS CoV-2 spike protein mutations. *Proteins: Struct., Funct., Bioinf.* **2021**, *89*, 569−576.

(49) Chatterji, A.; Ochoa, W. F.; Paine, M.; Ratna, B. R.; Johnson, J. E.; Lin, T. New addresses on an addressable virus nanoblock; uniquely reactive Lys residues on cowpea mosaic virus. *Chem. Biol.* **2004**, *11*, 855−863.

(50) Cai, H.; Shukla, S.; Wang, C.; Masarapu, H.; Steinmetz, N. F. Heterologous prime-boost enhances the antitumor immune response elicited by plant-virus-based cancer vaccine. *J. Am. Chem. Soc.* **2019**, *141*, 6509−6518.

(51) Wirth, D. M.; Pokorski, J. K. Design and fabrication of a low-cost pilot-scale melt-processing system. *Polymer* **2019**, *181*, 121802.

(52) Shao, S.; Ortega-Rivera, O. A.; Ray, S.; Pokorski, J. K.; Steinmetz, N. F. A scalable manufacturing approach to single dose vaccination against HPV. *Vaccines* **2021**, *9*, 66.

(53) Ortega-Rivera, O. A.; Pokorski, J. K.; Steinmetz, N. F. A single-dose, implant-based, trivalent virus-like particle vaccine against "cholesterol checkpoint" proteins. *Adv Ther.* **2021**, 2100014.

(54) Le, D. H. T.; Hu, H.; Commandeur, U.; Steinmetz, N. F. Chemical addressability of potato virus X for its applications in bio/nanotechnology. *J. Struct. Biol.* **2017**, *200*, 360−368.

(55) Mao, C.; Beiss, V.; Fields, J.; Steinmetz, N. F.; Fiering, S. Cowpea mosaic virus stimulates antitumor immunity through recognition by multiple MYD88-dependent toll-like receptors. *Biomaterials* **2021**, *275*, 120914.

(56) Mohsen, M. O.; Augusto, G.; Bachmann, M. F. The 3Ds in virus-like particle based-vaccines: design, delivery and dynamics. *Immunol. Rev.* **2020**, *296*, 155−168.

(57) Bachmann, M. F.; Jennings, G. T. Vaccine delivery: a matter of size, geometry, kinetics and molecular patterns. *Nat. Rev. Immunol.* **2010**, *10*, 787−796.

(58) Shukla, S.; Myers, J. T.; Woods, S. E.; Gong, X.; Czapar, A. E.; Commandeur, U.; Huang, A. Y.; Levine, A. D.; Steinmetz, N. F. Plant viral nanoparticles-based HER2 vaccine: immune response influenced by differential transport, localization and cellular interactions of particulate carriers. *Biomaterials* **2017**, *121*, 15−27.

(59) Huo, J.; Zhao, Y.; Ren, J.; Zhou, D.; Duyvesteyn, H. M. E.; Ginn, H. M.; Carrique, L.; Malinauskas, T.; Ruza, R. R.; Shah, P. N. M.; Tan, T. K.; Rijal, P.; Coombes, N.; Bewley, K. R.; Tree, J. A.; Radecke, J.; Paterson, N. G.; Supasa, P.; Mongkolsapaya, J.; Screaton, G. R.; Carroll, M.; Townsend, A.; Fry, E. E.; Owens, R. J.; Stuart, D. I. Neutralization of SARS-CoV-2 by Destruction of the Prefusion Spike. *Cell Host and Microbe* **2020**, *28*, 445−454.e6.

(60) Jallow, S.; Leligdowicz, A.; Kramer, H. B.; Onyango, C.; Cotten, M.; Wright, C.; Whittle, H. C.; Mcmichael, A.; Dong, T.; Kessler, B. M.; Rowland-Jones, S. L. The Presence of Prolines in the Flanking Region of an Immunodominant HIV-2 Gag Epitope Influences the Quality and Quantity of the Epitope Generated. *Eur. J. Immunol.* **2015**, *45*, 2232−2242.

(61) Watanabe, Y.; Berndsen, Z. T.; Raghwani, J.; Seabright, G. E.; Allen, J. D.; Pybus, O. G.; McLellan, J. S.; Wilson, I. A.; Bowden, T. A.; Ward, A. B.; Crispin, M. Vulnerabilities in coronavirus glycan shields despite extensive glycosylation. *Nat. Commun.* **2020**, *11*, 2688.

(62) Watanabe, Y.; Allen, J. D.; Wrapp, D.; McLellan, J. S.; Crispin, M. Site-specific glycan analysis of the SARS-CoV-2 spike. *Science* **2020**, *369*, 330−333.

N

(63) Zheng, Y.; Lee, P. W.; Wang, C.; Thomas, L. D.; Stewart, P. L.; Steinmetz, N. F.; Pokorski, J. K. Freeze-drying to produce efficacious CPMV virus-like particles. *Nano Lett.* **2019**, *19*, 2099−2105.

(64) Wen, A. M.; Lee, K. L.; Yildiz, I.; Bruckman, M. A.; Shukla, S.; Steinmetz, N. F. Viral nanoparticles for in vivo tumor imaging. *J. Visualized Exp.* **2012**, *69*, No. e4352.

(65) Shukla, S.; Jandzinski, M.; Wang, C.; Gong, X.; Bonk, K. W.; Keri, R. A.; Steinmetz, N. F. A viral nanoparticle cancer vaccine delays tumor progression and prolongs survival in a HER2+ tumor mouse model. *Adv Ther.* **2019**, *2*, 1800139.

(66) Reed, L. J.; Muench, H. A simple method of estimating fifty percent endpoints. *Am. J. Hyg.* **1938**, *27*, 493−498.